Journal of Aerosol Science 109 (2017) 28–37

Contents lists available at ScienceDirect

Journal of Aerosol Science

journal homepage: www.elsevier.com/locate/jaerosci

Quantification of branching in fumed silica

Andrew Mulderig[a], Gregory Beaucage[a,*], Karsten Vogtt[a], Hanqiu Jiang[a], Vikram Kuppa[b]

[a] Department of Materials Science, University of Cincinnati, Cincinnati, OH 45221, USA
[b] Nonstructural Materials Division, University of Dayton Research Institute, Dayton, OH 45469, USA

ARTICLE INFO

Keywords:
Fumed silica
Fractal
Aerosol
Small-angle x-ray scattering
Colloid
Aggregate

ABSTRACT

The fractal structure of ceramic aggregates has been widely studied in terms of the mass fractal dimension and primary particle size. However, there has not yet been a quantitative description of the branched topology in these structures. In this work, the highly ramified aggregate structure in six commercial grades of hydrophilic fumed silica is investigated. Ultra-small angle X-ray scattering was coupled to a hierarchical scattering model, the unified scattering function, to obtain topological parameters. These generic topological parameters were used to quantify branching and were then compared with simple aggregation simulations. Surprisingly, a single parameter, the sticking probability, can empirically account for complex topological differences in the materials studied. It is found that samples of higher specific surface area display a higher branch fraction. For grades of highest specific surface area, a hyper-branched structure is observed with extensive branch on branch aggregation. This approach can be used to quantify complex morphological differences in ceramic oxide and carbon black aggregates.

1. Introduction

The branched mass fractal structure of fumed silica offers high specific surface area that results in many of its commercially important reinforcement and rheological properties (Aranguren, Mora, DeGroot Jr., & Macosko, 1992; Pratsinis, 1998; Schaefer & Hurd, 1990; Schaefer, Oliver, Hurd, & Beaucage, 1991; Sternstein & Zhu, 2002; Witten, Rubenstein, & Colby, 1993; Witten & Sander, 1983). Flame aerosol synthesis of fumed silica allows particle size and, therefore, specific surface area, of the aggregates to be controlled. In commercial flame hydrolysis of fumed silica, $SiCl_4$, H_2 and dry air are mixed, injected into a burner and vaporized in the flame where fumed silica particles are formed. $SiCl_4$ is oxidized in the air and byproduct HCl is formed. SiO_2 molecules form clusters that grow in size due to coagulation and surface reactions. Following the high-temperature zone, clusters continue to coagulate to form primary particles. As the process continues, silica particles cool to a point at which primary particle growth by coalescence slows. As the product cools, coalescence no longer occurs but primary particles sinter together to form hard aggregates. The hard aggregates then assemble into soft agglomerates that are able to break apart and reform. Downstream, the product is cooled and byproduct HCl is separated from the fumed silica (Heine & Pratsinis, 1998; Schaefer & Hurd, 1990; Witten & Sander, 1983).

By tuning several parameters such as process temperature, particle residence time, precursor concentration and applied electric field, the primary particle size and, therefore, aggregate properties may be controlled. Grades of fumed silica are typically specified (and named) according to their surface to mass ratio (specific surface area). The specific surface area is mainly determined by the primary particle size and not by aggregate structure and size. The primary particle size and aggregate size of silica produced by flame

* Corresponding author.
E-mail address: gregory.beaucage@uc.edu (G. Beaucage).

http://dx.doi.org/10.1016/j.jaerosci.2017.04.001
Received 5 January 2017; Received in revised form 16 March 2017; Accepted 28 April 2017
Available online 28 April 2017
0021-8502/ © 2017 Elsevier Ltd. All rights reserved.

hydrolysis typically follow log-normal distributions. Polydispersity in primary particles is characterized by the geometric standard deviation (Beaucage, Kammler, & Pratsinis, 2004; Pratsinis, 1998), σ_g, while polydispersity in aggregate size can be conveyed in the polydispersity factor, C_p (Sorensen, 2001).

Fumed silica's valued reinforcement and rheological properties are derived from its primary particle and aggregate structure (Aranguren et al., 1992; Beaucage et al. 2004; Boldridge, 2010; Pratsinis, 1998; Schaefer & Hurd, 1990; Schaefer et al., 1991; Sternstein & Zhu, 2002; Witten et al. 1993). There have been few literature accounts that quantitatively describe the aggregate structure except in terms of analysis of TEM micrographs with qualitative descriptions such as classification into coarse and fine aggregates. Yet, there has been extensive description in terms of the mass-fractal dimension, which is related to the convolution and the branching of the aggregate. Since growth mechanisms can favor branch formation or extended linear chain growth, it is advantageous to distinguish between these two morphologies. Characterizing aggregate morphology is critical for prediction of the mobility of aggregates. For instance, disk shaped particles will have a dramatically different particle mobility compared to a linear chain of similar mass in a random conformation despite having identical mass fractal dimensions of 2 (Witten et al. 1993). The rheological enhancement and mechanical reinforcement are expected to display similar dependences on branch content of the aggregates (Beaucage, 2004; Rai et al., 2012).

Nanostructured aggregates can be described by their mass using a centrifugal particle mass analyzer (CPMA) or by their mobility using a differential mobility analyzer (DMA). Direct imaging techniques such as transmission electron microscopy (TEM) and scanning electron microscopy (SEM) are used to produce images of a small number of polydisperse aggregates and agglomerates. A large sample size is required to reach representative values for a given sample (Schaefer & Hurd, 1990). Generally, microscopy yields a 2-D projection of the 3-D aggregate structure. However, for fractal structures with dimensions greater than 2, a 2-D projection cannot access details of the ramified structure.

Quantification of branching requires a definition of terms associated with a branched structure (Beaucage, 2004; Ramachandran et al., 2009). In the simplest case, the average number of branches in an average aggregate, n_{br}, can be considered. These branches will have an average length, z_{Br}, in terms of the number of primary particles per branch. It is important to quantify the extent of branch-on-branch structure by the number of inner segments, n_i. Inner segments are segments of the structure terminated at both ends by branch points. The mole fraction of branches in the aggregate relative to the entire structure, ϕ_{br}, provides a simple and useful measure to compare aggregates with different degrees of aggregation (Beaucage, 2004; Rai et al., 2012; Ramachandran et al., 2009). Yet, ultimately, more abstract descriptors become necessary to provide detailed topological characterization of the aggregate structure. For example, the average conductive path length (minimum path) through a structure, p, can be described in terms of the number of primary particles in a minimum path (Herrmann & Stanley, 1988). The mass fractal dimension of the branched aggregate, d_f, describes the relationship between overall size, R, and aggregate mass, $z=(R/d_p)^{df}$. Aggregate size is normalized by the Sauter mean diameter, $d_p=6(V/S)$, of the primary particles to aid comparison among different aggregates. The minimum path, p, is related to R by $p=(R/d_p)^{d_{min}}$ where d_{min} describes the tortuosity of the minimum path. A connectivity dimension, $c=d_f/d_{min}$, can be defined such that it relates z and p via $z=p^c$. For a linear chain structure, c is 1; however, c approaches d_f in highly branched structures (Beaucage, 2004; Rai et al., 2012; Ramachandran et al., 2009). A schematic planar representation of an aggregate is shown in Fig. 1. Although it is possible to define these parameters using micrographs of individual aggregates or from simulations, such analysis is absent from the literature.

Small-angle X-ray scattering measurements offer a statistical approach to characterize the nanostructured branched aggregates and a direct measure of the mass-fractal parameters described in the previous paragraph. The probe size in scattering experiments depends on the wavelength, λ, and the scattering angle, θ; for nanoscale materials, X-rays and neutrons are used. In scattering experiments, wavelength and scattering angle are typically expressed with the momentum transfer vector, q, shown in Eq. (1).

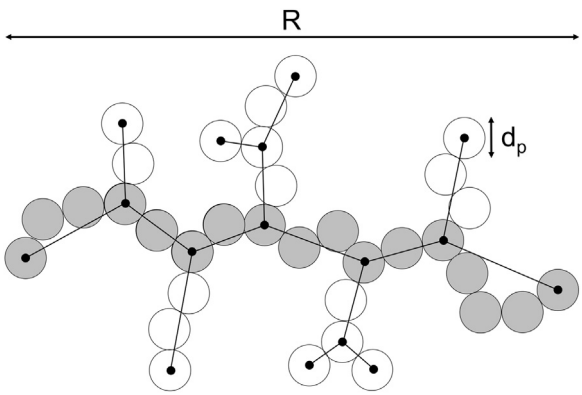

Fig. 1. Schematic representation of a planar mass fractal aggregate of size R consisting of z particles of diameter d_p. Primary particles along the minimum path, p, are shaded; the tortuosity of this minimum path is described by d_{min}. Black lines show the connective path, s, between branch points and endpoints, shown as black dots; this connective map may be used to determine the connectivity dimension, c. From the figure it can be counted that: z = 34 (all circles); p = 17 (grey circles); R = 13 (effective number of circles to span the aggregate); and calculated that $d_f=\log(34)/\log(13)=1.4$; $d_{min}=\log(17)/\log(13)=1.1$; $c=1.4/1.1=1.2$; $s=34^{1/1.2}=19$. (In 2-D d_f, d_{min}, and c must be less than or equal to 2.).

$$q = \frac{4\pi}{\lambda}\sin\left(\frac{\theta}{2}\right) \tag{1}$$

Small-angle scattering measurements probe real-space nanoscale structure through reciprocal-space measurements. Therefore, small structural features will be apparent in the high-q regime while larger structures will be probed at low q. The size of the structure being probed is roughly equal to $2\pi/q$. The unified scattering function, shown in Eq. (2), was used to fit reduced, desmeared X-ray scattering data across multiple hierarchical structural levels (Beaucage, 1995; Beaucage, 1996).

$$I(q) = \sum_{i=1}^{n}\left\{G_i e^{-\frac{q^2R_{g,i}^2}{3}} + e^{-\frac{q^2R_{g,i+1}^2}{3}} B_i q^{*-P_i}\right\}$$
$$q^* = \frac{q}{\mathrm{erf}\left(\frac{kqR_{g,i}}{\sqrt{6}}\right)^3} \tag{2}$$

The Unified scattering function applies Guinier's Law and a power law at each structural level to characterize the sample across multiple length scales. In this notation, $i = 1$ denotes the smallest structural level with higher values of i describing larger structures. Guinier's law, the first term in Eq. (2), allows the size of the scattering particles at structural level i to be described by their radius of gyration, $R_{g,i}$. The power law, the second term in Eq. (2), describes the internal or surface structure of the scattering particles. For smooth, dense particles the power law exponent, P_i, is 4 at hierarchical level $i = 1$ while $1 \leq P_i \leq 3$ indicates a mass fractal structure at hierarchical level $i = 2$. q^* accommodates the transition from one structural level to the next in hierarchical structures (Beaucage, 1995; Beaucage, 1996). The constant k has a value of 1.06 for most mass-fractals and a value of 1 for 3d levels.

Being a mass fractal aggregate, fumed silica displays three distinct hierarchical structural levels. From shortest to longest length scales, the first level pertains to primary particles, the second level describes the mass fractal aggregate structure and the third level consists of the agglomerate structure. The smallest two levels of this hierarchical structure are of particular interest in this work since the ramified structure in fumed silica is defined by the primary particles and the mass fractal aggregate structure. The size scale of the agglomerate structure is larger than that which may be reasonably probed by the USAXS measurement; agglomerate structure may be determined through light scattering measurements but this is beyond the scope of this work (Beaucage, 1995; Beaucage, 1996; Schaefer, Martin, Wiltzius, & Cannell, 1984; Sorensen, 2001).

Parameters obtained through fits to the Unified scattering function may be used to calculate topological quantities of the mass fractal aggregates using methods found in the literature (Beaucage, 1995; Beaucage, 1996). These include aggregate size (R), Sauter mean diameter (d_p), degree of aggregation (z), minimum path (p), connective dimension (c), tortuosity (d_{min}) and connective path (s) where $s = z^{1/c}$. The Sauter mean diameter, d_p, is the diameter of a sphere of similar surface to volume ratio as the scattering particle and gives a reasonable measure of primary particle size identical to that found from gas adsorption measurements. The degree of aggregation, z, describes the number of primary particles in an aggregate. The minimum path, p, is the number of primary particles in a short-circuit percolation pathway through the aggregate. The connective dimension, c, indicates the degree of branching of primary particles in the aggregate. The tortuosity dimension or minimum dimension, d_{min}, describes the fractal dimension of the minimum path, p. The number of primary particles on the connective or stick figure path between end points and branch points defines the connective path, s. These topological parameters may be derived from the scattering data and are used to describe mass fractal aggregates. These parameters are linked through Eq. (3) (Beaucage, 2004; Rai et al., 2012) and $d_f = c\, d_{min}$.

$$R = \frac{R_g}{d_p} = z^{1/d_f} = p^{1/d_{min}} = s^{1/c} \tag{3}$$

The topological parameters for mass fractal aggregates, introduced above, enable computation of quantities to define branching such as the branch fraction (ϕ_{br}), number of branches along the minimum path ($n_{br,p}$), number of branches in the aggregate (n_{br}), number of inner segments (n_i) and weight of branches (z_{br}). Branch fraction describes the proportion of primary particles in the aggregate which do not lie on the minimum path and is calculated by Eq. (4) (Beaucage, 2004; Rai et al., 2012).

$$\phi_{br} = \frac{z - p}{p} \tag{4}$$

The number of branches along the minimum path may be calculated via Eq. (5) under the assumption that each self-similar segment has an intrinsic fractal dimension of 1.8, as is the case for diffusion-limited aggregates (Beaucage, 2004; Ramachandran et al., 2009; Rai et al., 2012).

$$n_{br,p} = \left[p^{\left(\frac{1}{d_{min}} - \frac{5}{9}\right)}\right]^{\frac{9}{4}} - 1 \tag{5}$$

Similarly, the number of branches in the whole aggregate is determined by Eq. (6). Here it is assumed that the average functionality of each branch point, f, is three. In the absence of additional information, this assumption is generally reasonable (Rai et al., 2012).

$$\mathbf{n_{br}} = \frac{\mathbf{z}^{\left[\left(\frac{9}{4df}-\frac{5}{4c}\right)+\left(1-\frac{1}{c}\right)\right]} - \mathbf{1}}{\mathbf{f} - \mathbf{1}} \tag{6}$$

Aggregate segments that begin and end on branch points are called inner segments. The number of inner segments is determined using Eq. (7) (Rai et al., 2012).

$$\mathbf{n_i} = \mathbf{n_{br}} - \mathbf{n_{br,p}} \tag{7}$$

The number of inner segments reflects the extent of "hyper-branched" or aggregate network structure. "Hyper-branched" mass fractal structure is also called branch-on-branch aggregation. Hyper-branched structures can display unique physical properties compared to conventionally branched or linear structures. In this work, literature methods are used to quantify branching in mass fractal aggregates of fumed silica following small-angle scattering measurements and these results are compared with calculated values from simulated aggregates (Rai et al., 2012). Simulation of aggregates with similar branched structure allows for a visualization of the scattering parameterization. Given that scattering yields 7 independent structural descriptors for a given aggregate, there are a limited number of such visualizations. It is assumed that the matching simulated structure is likely similar to the actual aggregate nanostructure despite the simulation program having no connection to the physical growth process discussed in the introduction. Under such an assumption it is important to understand which features are artifacts of the particular aggregate growth mechanism chosen to create the structure and which are directly related to the SAXS parameterization. Specifically, the monomer-cluster growth simulation, used in this paper, results in aggregates with an obvious center point whereas the actual silica aggregates generally do not.

2. Materials and methods

Six grades of Aerosil® fumed silica (Ox50, A90, A150, A200, A300 & A380) with specific surface areas of 50 m^2/g to 380 m^2/g, respectively, were obtained from Evonik Industries and used as received. Transmission electron microscopy (TEM) samples were prepared by dispersing silica in ethanol at 0.1 mg/mL via ultrasonication for 30 minutes followed by dropping samples onto formvar-coated TEM sample grids. TEM samples were imaged using a Zeiss Libra 120 TEM operated at 120 kV and micrographs were recorded using a Gatan digital imaging camera. Small angle scattering samples were prepared by dusting fumed silica powder onto Scotch® tape then covering the powder with a second piece of tape. Two pieces of Scotch® tape were used as the background. Sample thickness was measured using digital calipers to be several hundred microns. Ultra small-angle X-ray scattering (USAXS) measurements were performed on the X-ray Science Division's 9-ID-C beam line at the Advanced Photon Source (APS) at Argonne National Laboratory using a Bonse-Hart camera containing two channel-cut silicon crystals. This high-flux instrument allows nanostructure to be probed using a momentum transfer vector $0.0001\ \text{Å}^{-1} \le q \le 0.1\ \text{Å}^{-1}$. Small-angle X-ray scattering measurements in the $0.01\ \text{Å}^{-1} \le q \le 0.2\ \text{Å}^{-1}$ regime were performed using a pinhole SAXS camera. A computer interface is used to control these instruments. Both instruments were operated using 15 keV synchrotron radiation. The Indra package for Igor Pro was used to reduce and desmear the data from this series of commercial silicas (Ilavsky & Jemian, 2009; Ilavsky et al., 2009; Ilavsky et al., 2013).

3. Results & discussion

Fumed silica aggregates display three structural levels consisting of primary particles, mass fractal aggregates and agglomerates. Of these hierarchical levels, primary particle and mass fractal aggregate structure have the most impact on the properties and the performance of fumed silica and will be studied in more detail. Transmission electron microscopy was used to image the mass fractal aggregate structure of fumed silica, shown in Fig. 2.

The micrographs in Fig. 2 exhibit the branched fractal nature of fumed silica. In all samples, aggregates consist of polydisperse primary particles, following a log-normal distribution in particle size. The topological differences among the various grades of fumed silica become apparent from this image series. As specific surface area increases across the sample series, several trends are observed. Primary particle size (d_p) is inversely proportional to specific surface area and monotonically decreases from the Ox50 sample through the A380 sample. Interestingly, similar aggregate size is observed as particle size decreases because while primary particle size decreases monotonically, degree of aggregation (z) increases monotonically across the sample series. The increased degree of aggregation is accompanied by an increased degree of branching.

To quantify the branched mass fractal aggregate structure, samples of six grades of Aerosil® fumed silica were probed using USAXS and SAXS measurements. The Unified scattering function, shown in Eq. (2), was fit to the scattering data across these hierarchical levels. Ultra-small angle X-ray scattering data for fumed silica samples and an example Unified fit are shown in Fig. 3a and b, respectively. The data in Fig. 3a has been scaled so that the Porod regime at highest q overlaps. This allows a simple comparison of the primary particle size as seen by the knee in the scattering pattern at about $q = 0.01\ \text{Å}^{-1}$. The shift in the knee to higher q indicates smaller primary particles following Guinier's law. The fractal dimension is the negative of the slope in the mid-q region from 0.001 to $0.01\ \text{Å}^{-1}$. The parameters from fits of the Unified scattering function, Eq. (2), to the data shown in Table 1.

As expected, primary particle size, as reflected in the radius of gyration, $R_{g,1}$ in Table 1, decreases with increasing specific surface area. No such trend was observed in aggregate size, indicating that the aggregate size is independent of specific surface area. The surface to volume ratio can be extracted from small-angle scattering data through the power law prefactor, B_1. The primary particles were determined to be dense with smooth surfaces since the power law scaling of $P_1 = 4$ was observed, in accordance with Porod's Law. In the second structural level, fumed silica aggregates display a power law scaling of 1.7–2.0, consistent with a mass fractal

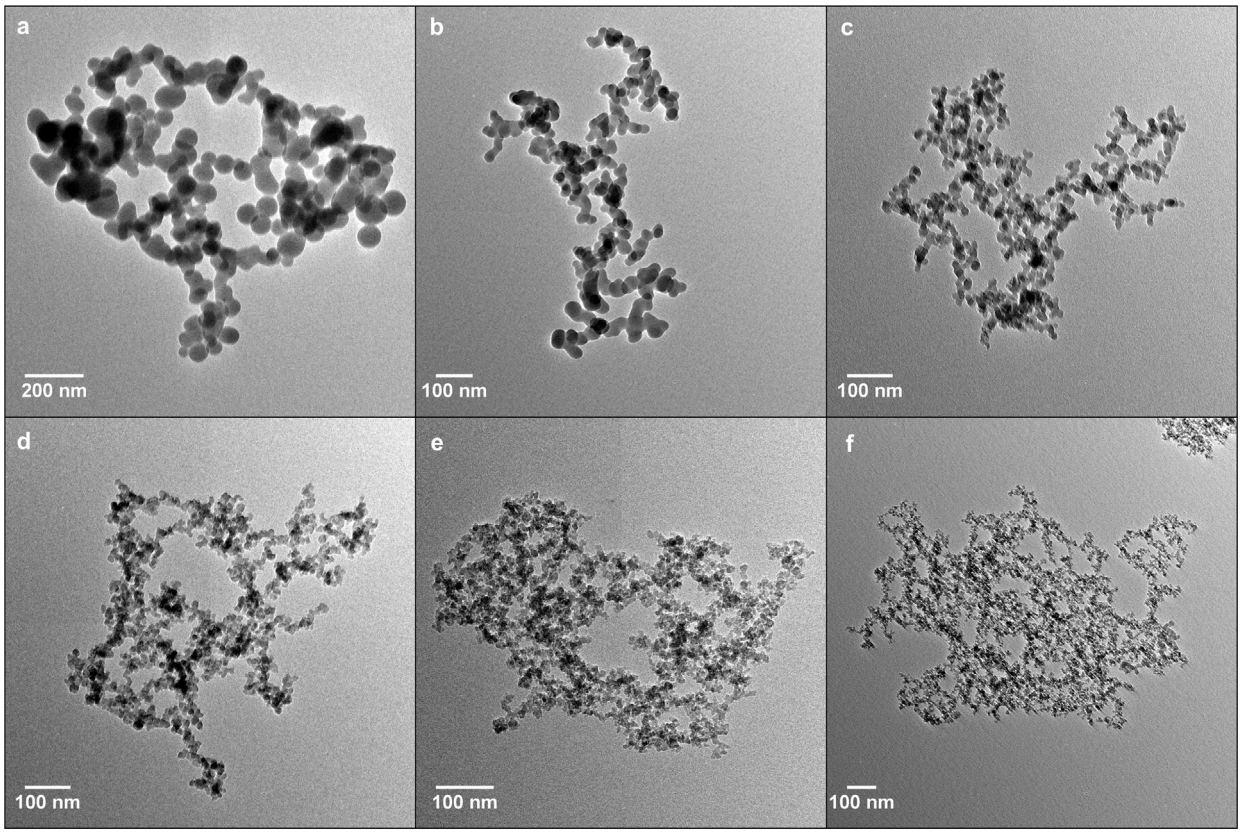

Fig. 2. Transmission electron micrographs of (a) Ox50, (b) A90, (c) A150, (d) A200, (e) A300 & (f) A380 samples showing branched fractal aggregate structure. Across this sample series of increasing specific surface area, primary particle size (d_p) decreased monotonically while significantly increased degree of aggregation (z) was observed.

aggregate structure. The agglomerate structure, level 3, is larger than that which can be measured by the USAXS instrument; therefore, only power law information is given for this level in Table 1.

As seen from the Unified fits to the scattering data, mass fractal aggregates in grades of higher specific surface area consisted of

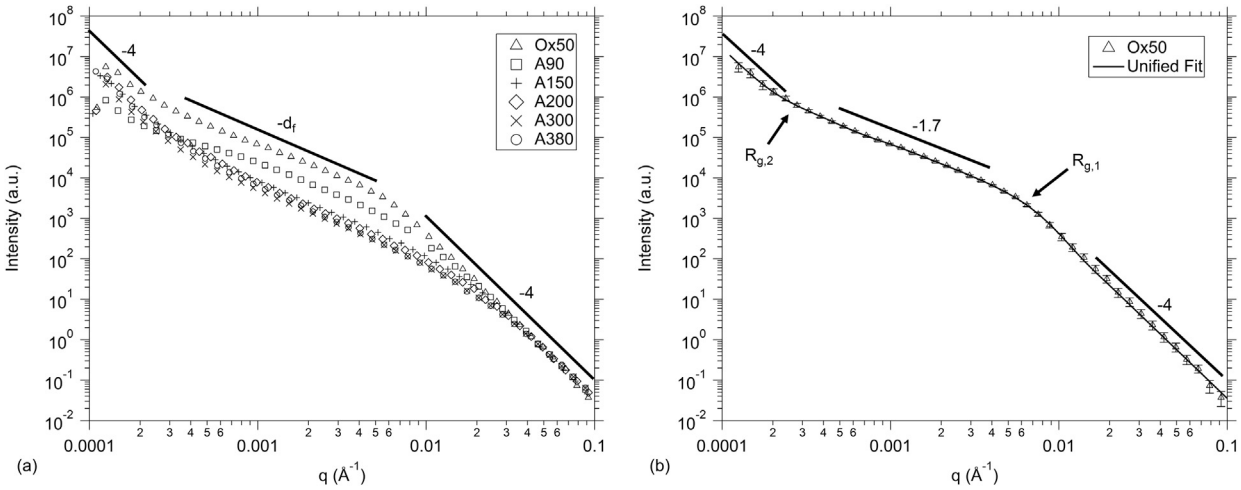

Fig. 3. (a) Ultra-small angle X-ray scattering data for a series of fumed silica samples. Scattering curves were scaled at high-q to emphasize the trend of decreasing primary particle size, determined from $R_{g,1}$, across grades of increasing specific surface area. (b) Unified scattering function fit to the scattering data for the Ox50 sample. Power law slopes and radii of gyration for primary particle (i = 1) and mass fractal (i = 2) hierarchical levels are noted. Seven independent parameters are obtained from the fit, the I(0) intercepts for the two Guinier regimes, G_1, G_2 and their corresponding R_g's, two power-law slopes and their prefactors, B_1 and B_2. The Porod slope at high-q results in a constraining equation allowing the calculation of the Sauter mean diameter, d_p. (The intensity is in arbitrary units because some of the curves were scaled and the thickness of the powders is difficult to specify.).

Table 1
Fitting parameters for Unified scattering function fit to USAXS data from fumed silica samples[a].

Sample	Ox50	A90	A150	A200	A300	A380
G_1 (r.u.)	4200 ± 200	7100 ± 600	1700 ± 300	420 ± 70	160 ± 40	70 ± 20
$R_{g,1}$ (Å)	300 ± 40	240 ± 40	220 ± 10	180 ± 10	130 ± 10	120 ± 10
B_1 ($\times 10^{-6}$ r.u.)	4.0 ± 0.3	32 ± 2	1.7 ± 0.1	9.5 ± 0.6	12 ± 0.9	7.2 ± 0.6
P_1	4	4	4	4	4	4
G_2 ($\times 10^3$ r.u.)	660 ± 30	1300 ± 20	800 ± 40	240 ± 80	130 ± 30	440 ± 20
$R_{g,2}$ ($\times 10^3$ Å)	4.5 ± 1.1	4.2 ± 1.0	4.9 ± 1.0	3.7 ± 1.1	3.4 ± 1.6	6.2 ± 1.1
B_2 ($\times 10^{-3}$ r.u.)	500 ± 70	120 ± 40	90 ± 30	23 ± 13	48 ± 12	18 ± 4
P_2	1.7 ± 0.1	1.7 ± 0.1	1.9 ± 0.1	2.0 ± 0.1	1.9 ± 0.1	2.0 ± 0.1
B_3 ($\times 10^{-9}$ r.u.)	1.9 ± 0.1	1.7 ± 0.1	4.1 ± 0.2	0.3 ± 0.1	1.7 ± 0.1	1.3 ± 0.1
P_3	4	4	4	4	4	4

[a] Relative units are listed because the thickness of the powders is subject to uncertainty but the values within a measurement for a given powder are relative to each other.

smaller primary particles, evidenced by the monotonically decreasing trend of d_p. The Sauter mean diameter is obtained from the surface to volume ratio from the scattering invariant. In Fig. 4, this surface to volume ratio is shown as a function of the specific surface area associated with the commercial silicas from the Evonik® specification sheets for hydrophilic fumed silicas. These values were obtained from gas adsorption measurements for general lots of these samples with a standard deviation that is shown in Fig. 4. The slope for a line in Fig. 4 reflects the silica density. Using the density of amorphous silica, 2.2 g/cm^3, the dashed line is obtained. This disagrees with the data from samples of higher nominal surface area per unit mass, which show a lower specific surface area. Such a reduction in density for high surface area oxides has been noted in the literature (Opalinska et al., 2015).

The parameterization of small-angle scattering data using the Unified scattering function allows an interpretation of the hierarchical structure in fumed silica. Moreover, the parameters obtained from fits to the scattering data may be used to derive quantities related to the branched mass fractal nature of these samples such as the degree of aggregation, z, minimum path, p, minimum dimension, d_{min}, connective dimension, c, branch fraction, ϕ_{br} and other parameters described by Eqs. (3)–(7). Polydispersity of primary particles (Beaucage et al. 2004) and aggregates (Sorensen, 2001) are quantified by σ_g and C_p, respectively, using literature methods.

Consistent with literature findings, aggregates in grades of higher specific surface area were also determined to have higher degrees of aggregation, z, shown in Table 2. When normalized by primary particle size, aggregate size, R, was generally seen to increase across grades of increasing specific surface area. However, the minimum path through the aggregates, p, only showed a marginal increase with increasing specific surface area. This means that as the aggregates grew larger the short circuit path through the aggregate became less convoluted. This result reflects changes in connectivity of the primary particles with decreased particle size. As primary particle size decreases across the series, the connectivity dimension of primary particles, c, was generally seen to increase, indicating higher branch content. This general trend was accompanied by increased fractal dimension, d_f, and decreased minimum dimension, d_{min}. These quantities are presented in Table 2.

Structural changes across the series of fumed silica samples of increasing specific surface area stem from increasing branch

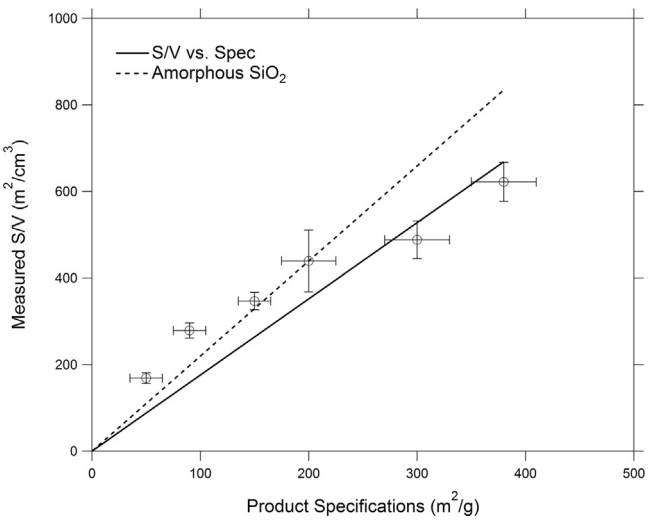

Fig. 4. Surface to volume ratio of fumed silica samples as measured by USAXS compared with the specific surface area, surface area per unit mass, from the product specifications. The slope of a line is the silica density and may vary with particle size. The dashed line reflects a density of 2.2 g/cm^3 for amorphous silica. The shallower line reflects a lower density that might occur for high surface area nanoparticles (Opalinska et al., 2015).

Table 2
Parameters describing aggregation and branching in Ox50, A90, A150, A200, A300 & A380 grades of fumed silica following analysis of USAXS data.

Sample	Ox50	A90	A150	A200	A300	A380
R	19	19	26	24	37	91
d_p (nm)	36	21	17	14	12	10
σ_g	1.43	1.54	1.60	1.59	1.52	1.58
C_p	1.54	1.53	1.51	1.50	1.52	1.51
z	157	177	483	567	819	6430
p	36	35	46	38	37	91
s	66	75	195	265	819	6430
d_{min}	1.21	1.20	1.17	1.14	1.00	1.00
c	1.41	1.46	1.62	1.75	1.86	1.95
d_f	1.70	1.75	1.90	1.98	1.86	1.95
$n_{br,p}$	8	8	12	13	36	91
n_i	11	15	56	93	373	3125
n_{br} (f = 3)	19	23	68	106	409	3215
z_{br} (f = 3)	15	17	37	40	22	71
ϕ_{br}, %	77	80	91	93	95	99

fraction, ϕ_{br}, the onset of hyper-branching and the presence of network aggregate structure in samples of highest specific surface area. Samples of Aerosil® A300 and A380 fumed silica contained hyper-branched mass fractal aggregates. The presence of hyper-branching is apparent in these samples from several quantities. Firstly, the connective paths, s, includes almost all primary particles, z, in the aggregates indicating that the aggregates have straight connections between branch points. Secondly, the number of branch points along the minimum paths is similar to the number of primary particles composing the minimum paths. This means that almost every particle contains a branch site. Thirdly, the high number of inner segments, n_i results in the number of branches, n_{br}, being half the number of primary particles (maximum number of branches for f = 3). The increase in hyperbranch content with specific surface area could be due to increased primary particle mobility during growth, with a transition from diffusion-limited growth to reaction-limited growth. This transition leads to gradual changes in both branching and convolution. The largest structural change seen is in the dramatic increase in hyperbranch content, indicated by n_i, for the aggregates as reaction limited growth begins to dominate. The branched and hyperbranched nature of fumed silica mass fractal aggregates is commercially important and may give rise to many of its properties and applications.

3.1. Simulation for visualization of aggregate structure

The fractal description from USAXS yields a rather detailed description of aggregate topology. From this description it is possible to manually construct a cartoon of the aggregate including the number of branches, branch length, degree of aggregation, minimum dimension, mass fractal dimension and the other parameters. One question is, can such a parameterization over 11 descriptors yield a structure that resembles “randomly” selected micrographs of a “representative” individual aggregate? Obviously the micrograph selection process and definition of representative are subject to question. In considering only the topology we have removed the main feature used to characterize fumed silica, the specific surface area and primary particle size.

Rather than drawing the aggregates, a simple diffusion limited monomer-cluster aggregation simulation was used with two input parameters, the degree of aggregation, z, and the sticking probability. The approach ignores the major growth processes involved in pyrolytic synthesis including sintering of the primary particles and aggregates, cluster-cluster growth, breaking of aggregates in shear streams, and mixing of aggregates from different growth conditions. Although we have measured the polydispersity of the primary particles, this is also ignored for simplicity in order to focus on topology. Surprisingly it was possible to match almost exactly the topology of the fumed silicas with the two parameters, sticking probability and degree of aggregation, even though the growth process in this simulation has no, or limited relationship to the actual formation process. This is partly a consequence of removing the primary particle size from this strictly topological consideration. The relevance of the sticking probability other than as an empirical parameter to match the data should be considered. The surprising result that two parameters can reproducibly produce aggregates made by a completely different and complex process suggests a universal constraint on the aggregates or at least a framework in which we can interpret complex growth phenomena in this case as making contributions to an effective sticking probability in the context of monomer-cluster growth.

The details of the simulation include use of a 3-D grid seeded with a single primary particle located at the origin (0, 0, 0) of the simulation box. New particles were introduced on one of the six walls (randomly chosen) of the simulation box at a random coordinate on the plane of the chosen wall. The new particle was allowed to randomly move one step in the x, y or z direction. If the particle moved outside of the simulation box, it was reintroduced on the opposite wall according to a periodic boundary condition. After each move, the program checked whether the new particle had moved to one of the 26 neighboring positions of any particle in the aggregate. The simulation box size was increased as more particles were added to the aggregate. Aggregate growth ceased once the model had added particles equal to the specified degree of aggregation, z. Primary particle size was normalized to one lattice site and a monodisperse particle size distribution was chosen to facilitate comparison among simulated aggregates and to simplify the procedure, respectively. This simulation illustrates possible examples of the mass fractal aggregate structures of the fumed silica

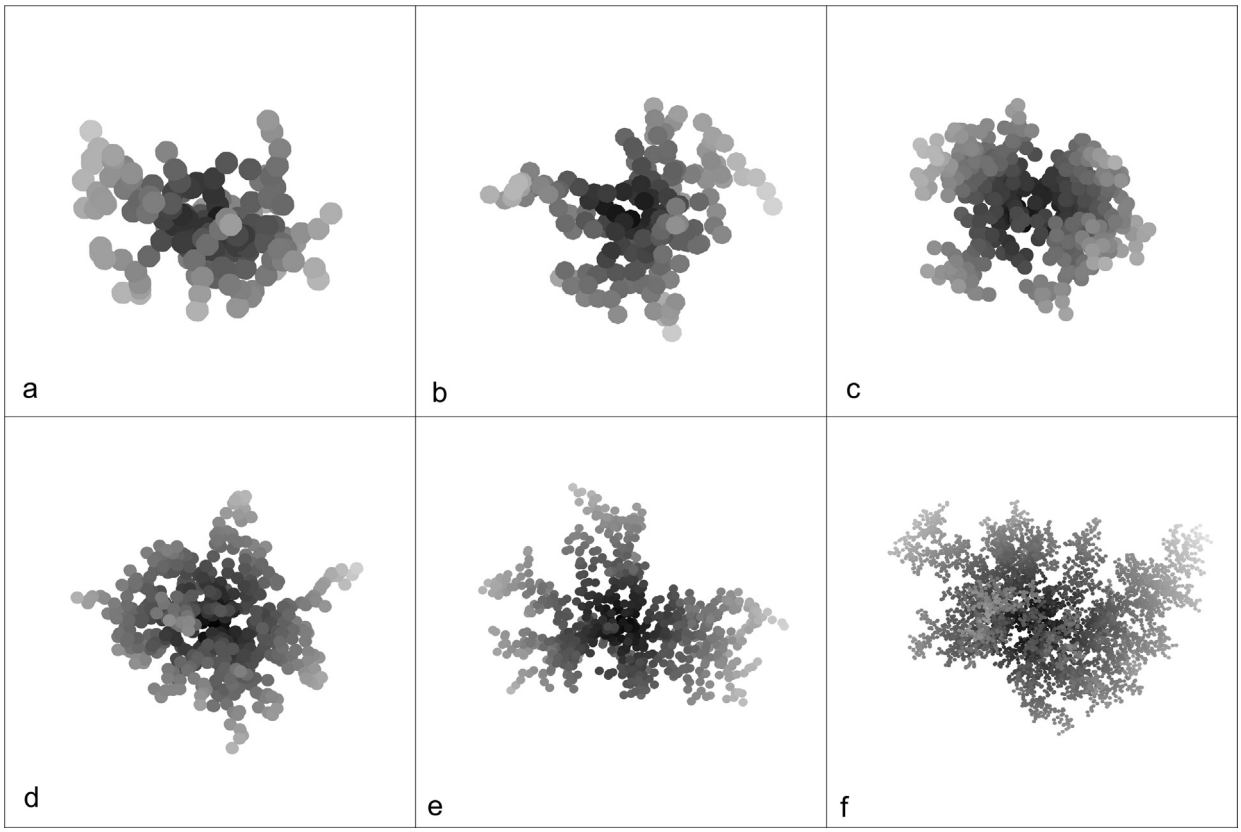

Fig. 5. Screen captures of aggregates simulated on a 3-D grid consisting of (a) z = 157, (b) 177, (c) 483, (d) 567, (e) 819 and (f) 6430.

samples for comparison with the TEM micrographs shown in Fig. 2. To match a specific silica, z was fixed and the sticking probability was adjusted by trial and error.

Simulated aggregates were analyzed using arguments and relations from the literature, including those presented in Eqs. (3)–(7) (Herrmann & Stanley, 1988; Meakin, Majid, Havlin, & Stanley, 1984; Witten & Sander, 1983). Since the minimum path is the mean short-circuit pathway through the aggregate, percolation pathways through the aggregate were determined and weight averaged to obtain p (Havlin & Ben-Avraham, 2002; Herrmann & Stanley, 1988). The end-to-end distance was calculated by weight averaging the distance between endpoints of the percolation pathways. Since z, p and d_f were known, all other parameters used to describe branching could be calculated. To replicate mass fractal aggregates in the fumed silica samples, sticking probability between 0.01 and 1.00 was chosen for simulated aggregates. Interestingly, sticking probability required for the simulated aggregates to match the fumed silica samples decreased across the sample series from z = 157 to z = 483 simulations but then increased going from z = 483 aggregates to z = 6430 aggregates, Table 3. This may indicate that the growth process for fumed silica aggregates of lower specific surface area is more reaction limited while aggregation of smaller primary particles is more diffusion limited.

The aggregates shown in Fig. 5 display similar branching characteristics compared to the target USAXS samples. Given that 7 independent branching parameters match between the simulated and actual aggregates, it is likely that the simulated structures bear close resemblance to the actual structures. Topological parameters obtained from analysis of these simulated aggregates are presented in Table 3 for comparison with the fumed silica samples. The simulation code used for aggregate formation and for quantification of the mass fractal structure according to Fig. 1 are given as Supplemental data.

4. Conclusion

The topological parameters defining branching for six grades of Aerosil® fumed silica were determined following analysis of ultra-small angle X-ray scattering measurements. The fumed silica samples in this work consisted of highly ramified mass fractal aggregates with samples of the highest specific surface area being hyper-branched network aggregates. Additionally, branched mass fractal aggregates were simulated and their topology was analyzed. Only two parameters, the degree of aggregation and the sticking probability, were used to model the aggregates. Topological parameters of the simulated aggregates were compared with results from scattering experiments and were found to be in good agreement. The ramified structure of fumed silica is critically important to its valuable reinforcement and rheological properties. Moreover, quantification of branching in fumed silica opens the door for predictive modeling in systems employing this important material. The approach is appropriate for other aggregate materials such as titania, zirconia, and carbon black.

Table 3
Parameters describing aggregation and branching in simulated mass fractal aggregates. Topological parameters calculated from simulated aggregates are in good agreement with SAXS results.

z	157	177	483	567	819	6430
Sticking probability	0.40	0.37	0.11	0.23	0.82	1.00
R	18	19	26	29	40	93
p	31	33	45	42	40	93
s	68	75	191	298	819	6430
d_{min}	1.2	1.2	1.17	1.11	1	1
c	1.47	1.48	1.62	1.7	1.82	1.93
d_f	1.76	1.75	1.9	1.89	1.82	1.93
$n_{br,p}$	8	8	12	17	39	92
n_i	14	18	56	104	370	3123
n_{br} (f = 3)	21	26	68	121	409	3215
z_{br} (f = 3)	17	18	37	30	20	69
ϕ_{br}, %	80%	81%	91%	93%	95%	99%

Acknowledgements

This work was supported by the National Science Foundation through grants CMMI-1635865 and CMMI-1636036.

Andrew Mulderig was supported by the Department of Energy through the DOE Office of Science Graduate Student Research Program.

Use of the Advanced Photon Source, an Office of Science User Facility operated for the U.S. Department of Energy (DOE) Office of Science by Argonne National Laboratory, was supported by the U.S. DOE under Contract No. DE-AC02-06CH11357. USAXS data was collected at the Advanced Photon Source on beam line 9-ID-C operated by the X-ray Science Division. We gratefully acknowledge the vital assistance of Jan Ilavsky and his staff at 9-ID-C.

Fabrication and imaging of transmission electron microscopy (TEM) samples was conducted at the Center for Nanophase Materials Sciences, which is a DOE Office of Science User Facility.

Sotiris Pratsinis of ETH Zurich provided samples and useful advice concerning this paper. He is gratefully acknowledged for his assistance with this work.

Appendix A. Supplementary material

Supplementary data associated with this article can be found in the online version at http://dx.doi.org/10.1016/j.jaerosci.2017.04.001.

References

Aranguren, M. I., Mora, E., DeGroot, J. V., Jr., & Macosko, C. W. (1992). Effect of reinforcing fillers on the rheology of polymer melts. *Journal of Rheology*, ***36***, 1165.
Beaucage, G. (1995). Approximations leading to a unified exponential/power-law approach to small-angle scattering. *Journal of Applied Crystallography*, ***28***, 717–728.
Beaucage, G. (1996). Small-angle scattering from polymeric mass fractals of arbitrary mass-fractal dimension. *Journal of Applied Crystallography*, ***29***, 134–146.
Beaucage, G. (2004). Determination of branch fraction and minimum dimension of mass-fractal aggregates. *Physical Review E – Statistical, Nonlinear, and Soft Matter Physics*, ***70***, 031401-1–031401-10.
Beaucage, G., Kammler, H. K., & Pratsinis, S. E. (2004). Particle size distributions from small-angle scattering using global scattering functions. *Journal of Applied Crystallography*, ***37***, 523–535.
Boldridge, D. (2010). Morphological characterization of fumed silica aggregates. *Aerosol Science and Technology*, ***44***, 182–186.
Havlin, S., & Ben-Avraham, D. (2002). Diffusion in disordered media. *Advances in Physics*, ***51***, 187–292.
Heine, M. & Pratsinis, S. High concentration agglomerate dynamics at high temperatures. Langmuir, 22, 10238–10245.
Herrmann, H. J., & Stanley, H. E. (1988). The fractal dimension of the minimum path in two- and three-dimensional percolation. *Journal of Physics A: Mathematical and General*, ***21***, L829–L833.
Ilavsky, J., & Jemian, P. R. (2009). Irena: Tool suite for modeling and analysis of small angle scattering. *Journal of Applied Crystallography*, ***42***, 347–353.
Ilavsky, J., Jemain, P. R., Allen, A. J., Zhang, F., Levine, L. E., & Long, G. G. (2009). Ultra-small-angle X-ray scattering at the advanced photon source. *Journal of Applied Crystallography*, ***42***, 469–479.
Ilavsky, J., Zhang, F., Allen, A. J., Levine, L. E., Jemain, P. R., & Long, G. G. (2013). Ultra-small-angle X-ray scattering instrument at the advanced photon source: History, recent development, and current status. *Metallurgical and Materials Transactions A*, ***44***, 68–76.
Meakin, P., Majid, I., Havlin, S., & Stanley, H. E. (1984). Topological properties of diffusion limited aggregation and cluster-cluster aggregation. *Journal of Physics A: Mathematical and General*, ***17***, L975–L981.
Opalinska, A., Malka, O., Dzwolak, W., Chudoba, T., Presz, A., & Lojkowski, W. (2015). Size-dependent density of zirconia nanoparticles. *Beilstein Journal of Nanotechnology*, ***6***, 27–35.
Pratsinis, S. (1998). Flame aerosol synthesis of ceramic powders. *Progress in Energy and Combustion Science*, ***24***, 197–219.
Rai, D., Beaucage, G., Jonah, E. O., Britton, D. T., Sukumaran, S., & Härting, M. (2012). Quantitative investigations of aggregate systems. *The Journal of Chemical Physics*, ***137***, 044311–1–044311-6.
Ramachandran, R., Beaucage, G., Kulkarni, A. S., McFaddin, D., Merrick-Mack, J., & Galiatsatos, V. (2009). Branch content of metallocene polyethylene. *Macromolecules*, ***42***, 4746–4750.
Schaefer, D. W., Martin, J. E., Wiltzius, P., & Cannell, D. S. (1984). Fractal geometry of colloidal aggregates. *Physical Review Letters*, ***52***, 2371–2374.

Schaefer, D. W., & Hurd, A. J. (1990). Growth and structure of combustion aerosols: Fumed silica. *Aerosol Science and Technology*, ***12***, 876–890.
Schaefer, D. W., Oliver, B. J., Hurd, A. J., Beaucage, G. B., Ivie, J. J., & Herd, C. R. (1991). Structure of combustion aerosols. *Journal of Aerosol Science*, ***22***, 5447–5450.
Sorensen, C. M. (2001). Light scattering by fractal aggregates: A review. *Aerosol Science and Technology*, ***35***, 648–687.
Sternstein, S. S., & Zhu, A.-J. (2002). Reinforcement mechanism of nanofilled polymer melts as elucidated by nonlinear viscoelastic behavior. *Macromolecules*, ***35***, 7262–7273.
Witten, T. A., & Sander, L. M. (1983). Diffusion-limited aggregation. *Physical Review B*, ***27***, 5686–5697.
Witten, T. A., Rubenstein, M., & Colby, R. H. (1993). Reinforcement of rubber by fractal aggregates. *Journal de Physique II*, ***3***, 367–383.